

Incompressible Newtonian Laminar Flows

4

4.1 Introduction and the basic equations

The problems of incompressible flows dominate a large part of the fluid mechanics scene. For this reason, they are given special attention in this book and we devote three chapters to this subject. In the present chapter we deal with various laminar steady-state and transient Newtonian situations in which the flow is forced by appropriate pressure gradients and boundary forces. In the next chapter we shall consider non-Newtonian flows including metal forming and viscoelastic flows. Free surface flows in which gravity establishes appropriate free surface patterns as well as the so-called buoyancy force in which the only driving forces are density changes caused by temperature variations are discussed in [Chapter 6](#).

It is mentioned in [Ref. \[1\]](#) that certain difficulties are encountered with incompressibility when this is present in the equations of solid mechanics. We shall find that exactly the same problems arise again in fluids especially with very slow flows where the acceleration can be neglected and viscosity is dominant (so-called Stokes flow). Complete identity with linear elasticity is found here.

The essential difference in the governing equations for incompressible flows from those of compressible flows is that the coupling between the equations of energy and the other equations is very weak and thus frequently the energy equations can be considered completely independently.

To proceed further we return to the original equations of fluid dynamics which have been given in [Chapters 1](#) and [3](#); we repeat these below for problems of small compressibility.

Conservation of mass

$$\frac{\partial \rho}{\partial t} = \frac{1}{c^2} \frac{\partial p}{\partial t} = - \frac{\partial U_i}{\partial x_i} \quad (4.1)$$

and $c^2 = K/\rho$ where K is the bulk modulus. Here in the incompressible limit, the density ρ is assumed to be constant and in this situation the term on the left-hand side is simply zero.

Conservation of momentum

$$\frac{\partial U_i}{\partial t} = - \frac{\partial}{\partial x_j} (u_j U_i) + \frac{\partial \tau_{ij}}{\partial x_j} - \frac{\partial p}{\partial x_i} + \rho g_i \quad (4.2)$$

In the above we define the mass flow fluxes as

$$U_i = \rho u_i \quad (4.3)$$

Conservation of energy

$$\frac{\partial(\rho E)}{\partial t} = -\frac{\partial}{\partial x_j}(u_j \rho E) + \frac{\partial}{\partial x_i} \left(k \frac{\partial T}{\partial x_i} \right) - \frac{\partial}{\partial x_j}(u_j p) + \frac{\partial}{\partial x_i}(\tau_{ij} u_j) \quad (4.4)$$

This is now uncoupled and can be solved independently. In the above u_i are the velocity components, E is the specific energy ($c_v T$), p is the pressure, T is the absolute temperature, ρg_i represents the body force and other source terms, and τ_{ij} are the deviatoric stress components given by (1.11b):

$$\tau_{ij} = \mu \left(\frac{\partial u_i}{\partial x_j} + \frac{\partial u_j}{\partial x_i} \right) \quad (4.5)$$

With the substitution made for density changes we note that the essential variables in the first two equations become those of pressure and velocity. In exactly the same way as these, we can specify the variables linking displacements and pressure in the case of incompressible solids. It is thus possible to solve these equations in one of many ways described in Chapter 10 of Ref. [1] though, of course, the use of the CBS algorithm is obvious.

Unless the viscosity and in fact the bulk modulus have a strong dependence on temperature the problem is very weakly linked with the energy equation which can be solved independently.

The energy equation for incompressible materials is best written in terms of the absolute temperature T avoiding the specific energy. The equation now becomes simply (neglecting source terms)

$$c_v \rho \left[\frac{\partial T}{\partial t} + u_j \frac{\partial T}{\partial x_j} \right] = \frac{\partial}{\partial x_i} \left(k \frac{\partial T}{\partial x_i} \right) + \frac{\partial}{\partial x_i}(\tau_{ij} u_j) - \frac{\partial}{\partial x_j}(u_j p) \quad (4.6)$$

and we note that this is now a scalar convection-diffusion equation of the type we have already encountered in [Chapter 2](#), written in terms of the variable temperature as the unknown. In the above equation, the last two work dissipation terms are often neglected for fully incompressible flows. Note that the above equation is derived assuming the density and c_v (specific heat at constant volume) to be constants.

In this chapter we shall in general deal with problems for which the coupling is weak and the temperature equations do not present any difficulties. However, in [Chapter 6](#) we shall encounter buoyancy effects caused by atmospheric or general circulation induced by small density changes due to temperature differences.

If viscosity is a function of temperature, it is very often best to proceed simply by iterating over a cycle in which the velocity and pressure are solved with the assumption of known viscosity, followed by the solution of temperature. Many practical problems have been so treated very satisfactorily. We shall show some of these applications in the field of metal forming in the next chapter.

In the main part of this chapter we shall consider the solution of viscous, Newtonian fluids and we shall generally use the CBS algorithm described in [Chapter 3](#), though

on occasion we shall depart from this due to the similarity with the equations of solid mechanics and use a more direct approach either by satisfying the BB stability conditions of Chapter 10 in [1] for the velocity and pressure variables, or by using reduced integration in the context of a pure velocity formulation with a penalty parameter.

4.2 Use of the CBS algorithm for incompressible flows

4.2.1 The fully explicit artificial compressibility form

The fully explicit scheme for incompressible flow approximation is obtained by substituting $0.5 \leq \theta_1 \leq 1.0$ and $\theta_2 = 0$ into Eqs. (3.56) and (3.59). It is obvious that $c \rightarrow 0$ in incompressible flow approximations and therefore needs to be replaced with an artificial parameter β as discussed in Section 3.5.1 [2,3]. With such an approximation, the steady-state solutions will be straightforward. However, for unsteady state the dual time-stepping procedure described in Section 3.5.2 needs to be followed. We consider both steady and unsteady state solutions here. The artificial compressibility-based CBS scheme is generally referred to as the CBS-AC scheme in the present text.

4.2.2 The semi-implicit form

For problems of incompressibility with K being equal to infinity or indeed when K is very large, we have a choice of using the fully explicit procedure with artificial compressibility as discussed in the above section and we have a second choice of using the CBS algorithm in its semi-implicit form with $0.5 \leq \theta_1 \leq 1.0$ and $0.5 \leq \theta_2 \leq 1$ (Chapter 3, Section 3.4.2) [4]. This of course will use an explicit solution for the momentum equation followed by solution of the pressure Laplacian form (the Poisson equation). The solution which has to be obtained implicitly involves only the pressure variable [Eq. (3.56)] and we will further notice that, from the contents of Chapter 3, at each step the basic equation remains unchanged and therefore the solution can be repeated simply with different right-hand side vectors.

The convergence rate to steady state of course depends on the time step used and here we have the time step limitation given by the Courant number

$$\Delta t_1 \leq \Delta t_{\text{crit}} = \frac{h}{|\mathbf{u}|} \quad (4.7)$$

for inviscid problems and for viscous problems

$$\Delta t_2 \leq \Delta t_{\text{crit}} = \frac{h^2}{2\nu} \quad (4.8)$$

is an additional limitation. Here we note immediately that the viscosity lowers the limit quite substantially and therefore convergence to steady state may not be exceedingly rapid. The examples which we shall show nevertheless indicate its good performance.

Example 4.1. Incompressible flow in a lid-driven cavity

The classical problem on which we shall judge the performance is that of the closed cavity driven by the motion of a lid [5–9]. There are various ways of assuming

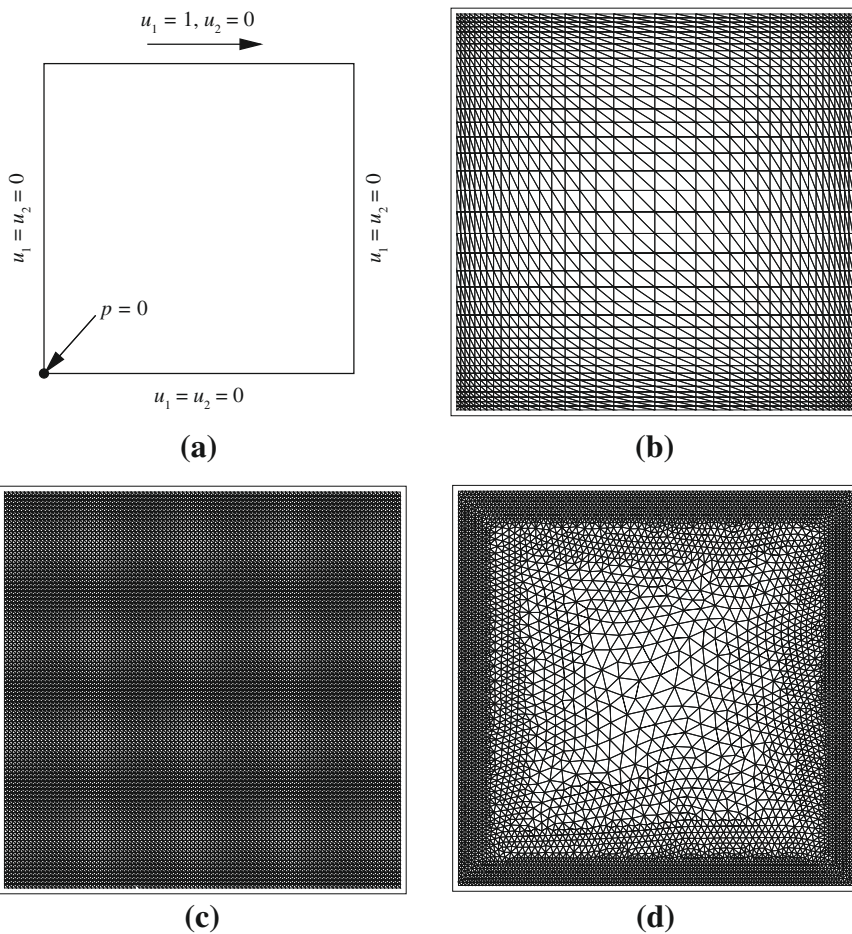
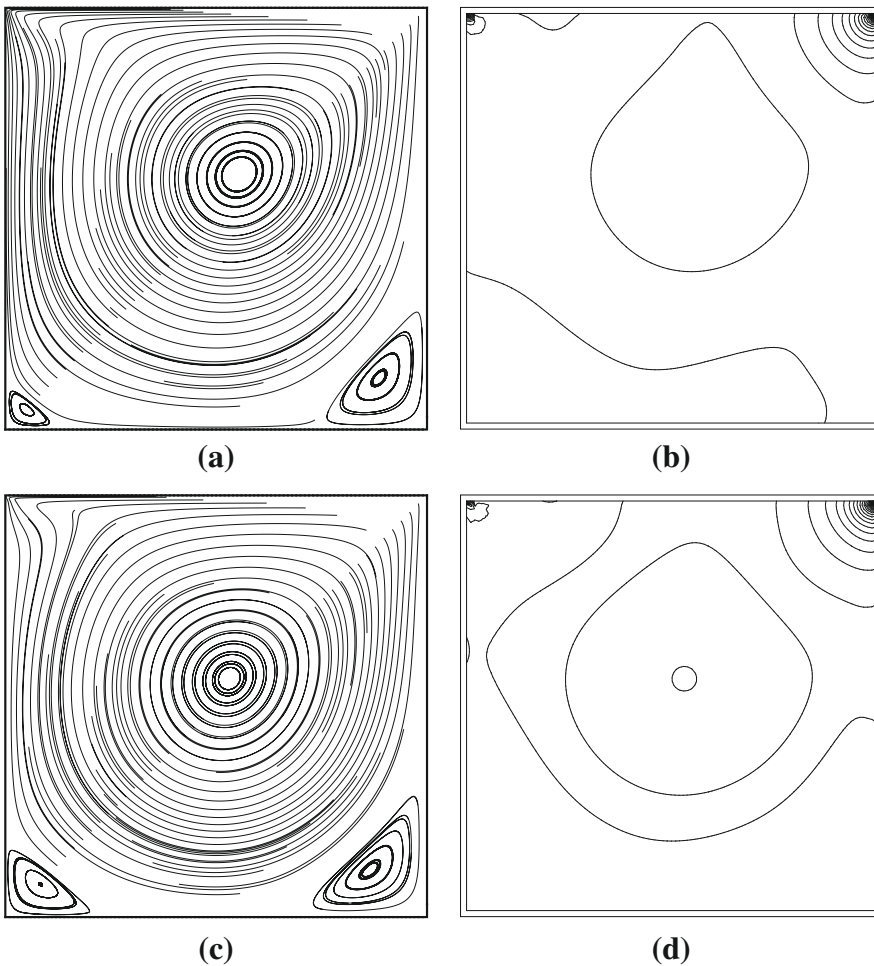


FIGURE 4.1

Incompressible flow in a lid-driven cavity. Geometry and meshes. (a) Geometry and boundary conditions; (b) nonuniform structured mesh (elements: 2888, nodes: 1521); (c) uniform structured mesh (elements: 20,000, nodes: 10,201); (d) nonuniform unstructured mesh (elements: 10,596, nodes: 5515).

the boundary conditions but the most common is one in which the velocity along the top surface increases from the corner node to the driven value in the length of one element (so-called ramp conditions).¹ The solution was obtained for different values of Reynolds number thus testing the performance of the viscous formulation.

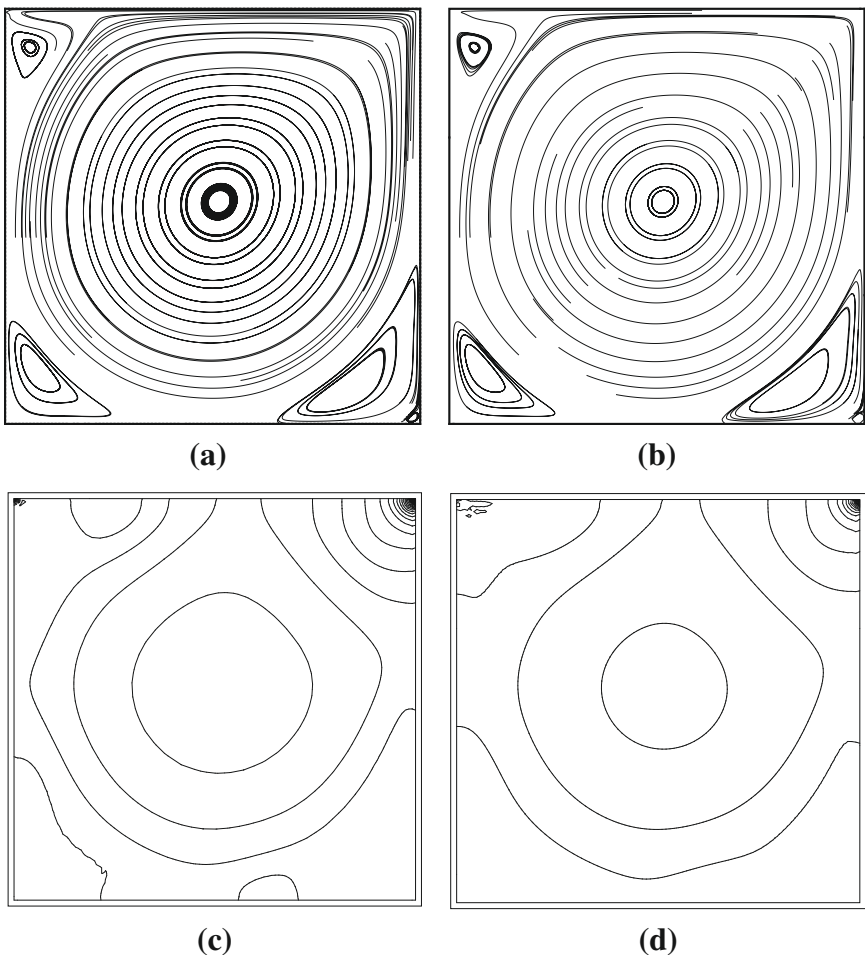
¹Some investigators use the leaking lid formulation in which the velocity along the top surface is constant and varies to zero within an element in the sides. It is preferable however to use the formulation where velocity is zero on all nodes of the vertical sides.

**FIGURE 4.2**

Incompressible flow in a lid-driven cavity: (a) $Re = 100$, stream traces; (b) $Re = 100$, pressure contours; (c) $Re = 400$, stream traces, (d) $Re = 400$, pressure contours.

The problem has been studied by many investigators but probably the most detailed early investigation was that of Ghia et al. [5] in which they quote many solutions and data for different Reynolds numbers. We shall use those results for comparison.

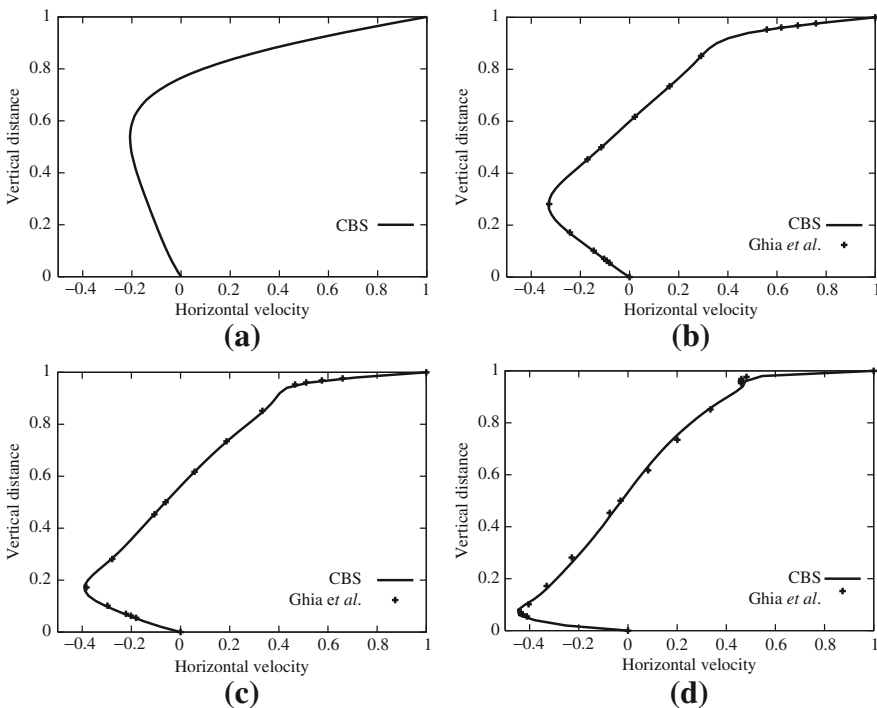
In the first figure, Fig. 4.1, we show the geometry, boundary conditions, and finite element meshes. The problem definition is shown in Fig. 4.1a. The top lid of the cavity is assumed to move with a prescribed velocity in one direction and all other walls are stationary. No-slip conditions for velocity are applied on all solid walls. Pressure is prescribed at one point as shown in Fig. 4.1a. Several meshes have been tested in the past [2] but only three meshes are shown in Fig. 4.1. The first mesh is

**FIGURE 4.3**

Incompressible flow in a lid-driven cavity: (a) $Re = 5000$, stream traces on the unstructured mesh; (b) $Re = 5000$, stream traces on the uniform structured mesh; (c) $Re = 5000$, pressure contours on the unstructured mesh; (d) $Re = 5000$, pressure contours on the uniform structured mesh.

a nonuniform structured mesh with smaller elements close to the walls. The second mesh is a uniform structured mesh of 100×100 size and the last mesh given in Fig. 4.1 is a nonuniform unstructured mesh with higher resolution close to the cavity walls.

Figure 4.2 shows the stream traces and pressure contours for $Re = 100$ and 400 generated from the unstructured mesh shown in Fig. 4.1d. As seen the results are smooth and free of oscillations. Expected secondary vortices on both bottom corners are predicted excellently by the scheme. In Fig. 4.3 the results produced by the

**FIGURE 4.4**

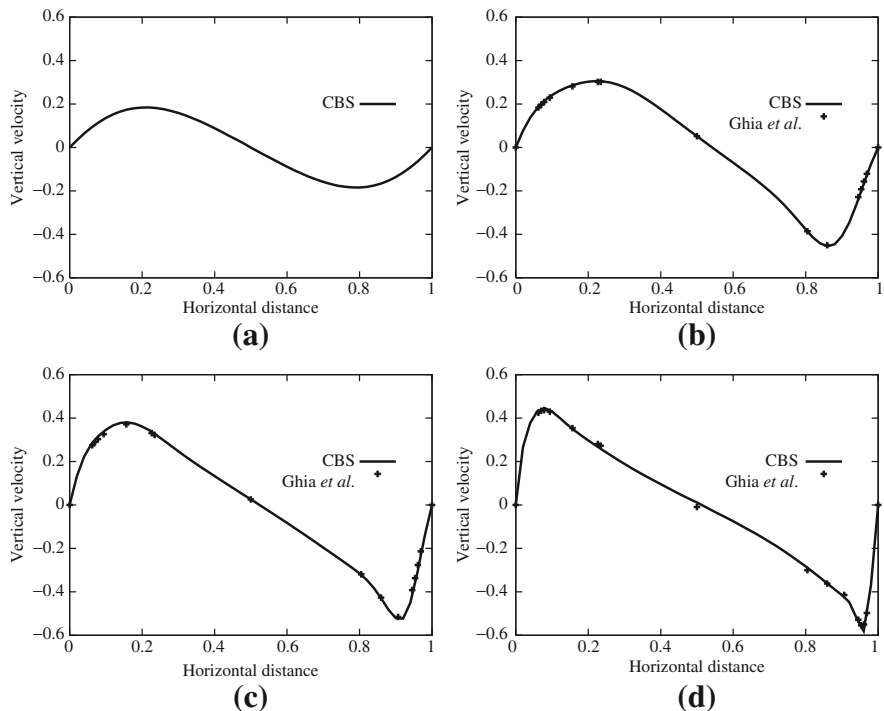
Incompressible flow in a lid-driven cavity. Horizontal velocity distribution at different Reynolds numbers: (a) $Re = 0$; (b) $Re = 400$; (c) $Re = 1000$; (d) $Re = 5000$.

unstructured mesh (Fig. 4.1d) and uniform structured mesh (Fig. 4.1c) are compared for a Reynolds number of 5000. As noticed both the results are smooth and in good agreement with the other reported results. The important aspect of this figure is that a small corner vortex at the bottom right corner, which normally requires a very high mesh resolution, has been predicted by the CBS scheme.

The horizontal and vertical velocity component distributions are shown in Figs. 4.4 and 4.5. All the results in these figures are produced using the unstructured mesh (Fig. 4.1d). As noted the results are in excellent agreement with the benchmark fine mesh (121×121) solutions reported by Ghia et al. [5].

A three-dimensional lid-driven cavity solution is shown in Fig. 4.6 at $Re = 400$. As seen the solutions obtained are smooth and the velocity distribution is in good agreement with the 2D results. However, it should be noted that at higher Reynolds numbers (>1000) no steady state exists and the results show a fully three-dimensional solution [3, 8, 9].

Figure 4.7 gives the steady-state convergence histories of the lid-driven cavity problem for semi-implicit and fully explicit schemes. The L_2 norm of velocity residual

**FIGURE 4.5**

Incompressible flow in a lid-driven cavity. Vertical velocity distribution at different Reynolds numbers: (a) $Re = 0$; (b) $Re = 400$; (c) $Re = 1000$; (d) $Re = 5000$.

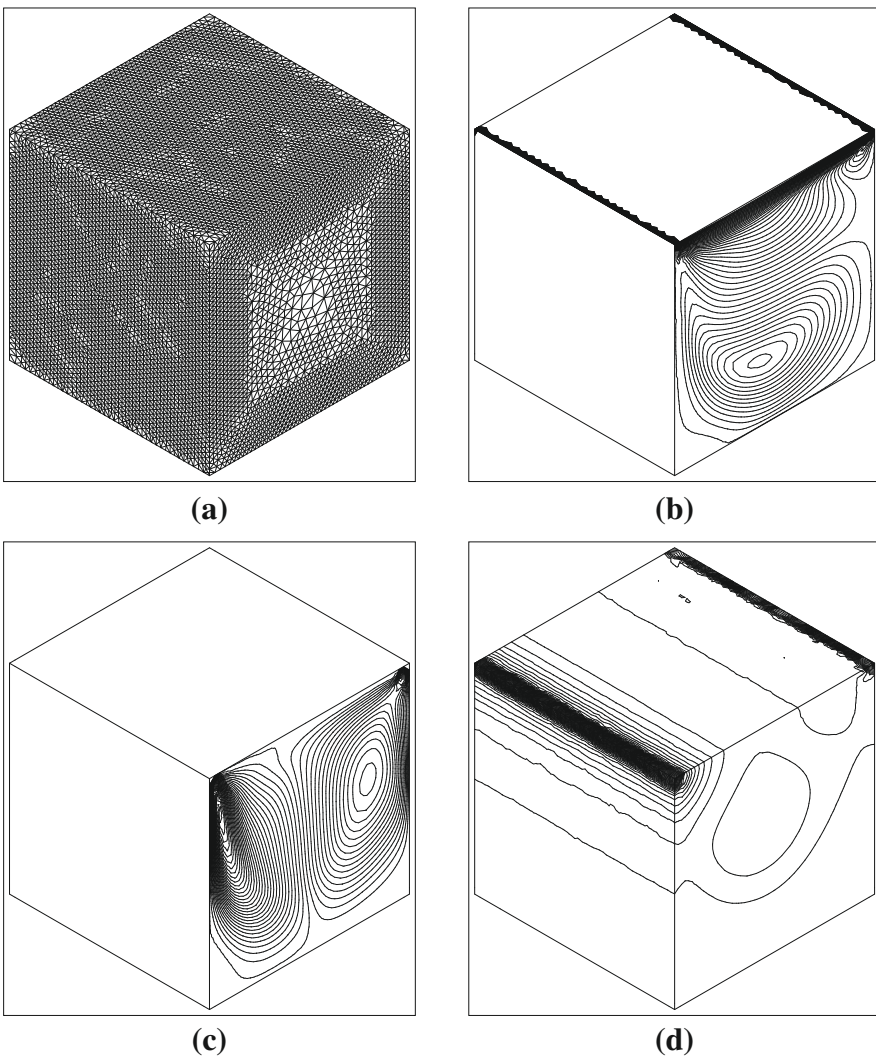
is calculated as

$$\frac{\sum_{i=1}^{No.\,Nodes} \sqrt{(|\mathbf{u}|^{n+1} - |\mathbf{u}|^n)^2}}{\sum_{i=1}^{No.\,Nodes} \sqrt{(|\mathbf{u}|^{n+1})^2}} \quad (4.9)$$

A steady state was assumed when the above L_2 norm reached a value below 10^{-5} . It is clear from Fig. 4.7 that both the fully explicit and semi-implicit schemes converge almost at the same rate at $Re = 5000$. However, at $Re = 400$, the convergence rate of the semi-implicit form is slightly better than that of the fully explicit scheme. Both the results were produced using local time stepping.

Example 4.2. Steady flow past a backward facing step

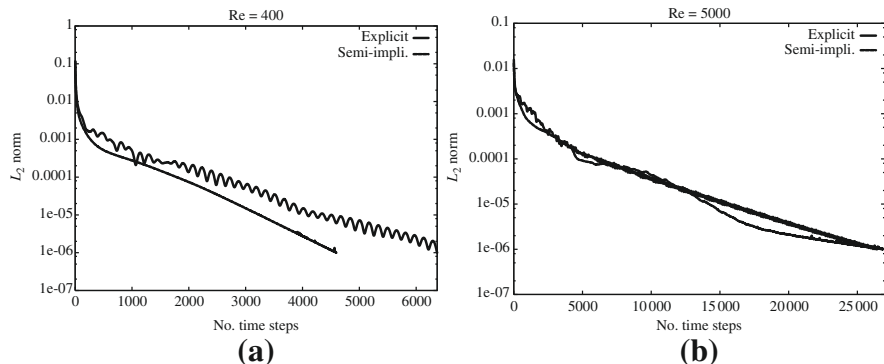
In this example, another widely used benchmark problem of flow past a backward facing step is considered [10]. The problem definition is shown in Fig. 4.8. The inlet is situated at a distance of four times the step height from the step. The inlet height is twice the height of the step itself. The total length is 40 times the height of the step. The inlet Reynolds number based on the step height and the average inlet velocity is 229.

**FIGURE 4.6**

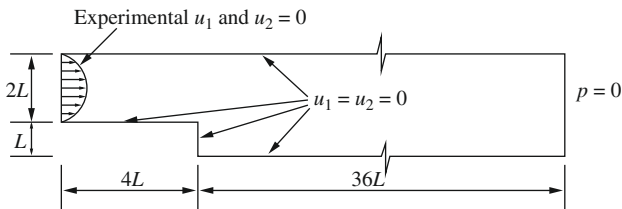
Incompressible flow in a 3D lid-driven cavity. Mesh and contours at $\text{Re} = 400$: (a) unstructured mesh; (b) u_1 contours; (c) u_3 contours; (d) pressure contours.

At the inlet a nearly parabolic horizontal velocity profile (experimental) is assumed and the vertical velocity component is assumed to be equal to zero. On the walls no-slip boundary conditions apply and at the exit constant (zero) pressure conditions are prescribed.

In Fig. 4.9, the unstructured mesh used and the contours of the horizontal velocity component and pressure are given. The mesh is finer near the walls and coarser away

**FIGURE 4.7**

Lid-driven cavity. Steady-state convergence histories for (a) $Re = 400$ and (b) 5000. Comparison between fully explicit and semi-implicit schemes.

**FIGURE 4.8**

Incompressible flow past a backward facing step. Geometry and boundary conditions.

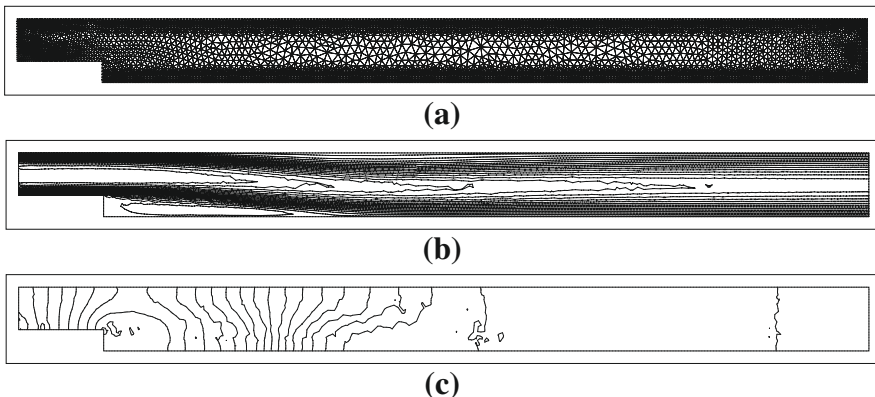
from the walls. The variable distribution shown in Fig. 4.9b and c is in good agreement with the available data.

In Fig. 4.10, the numerical data are compared against the experimental data in the recirculation zone. As seen the agreement between the numerical and experimental data [10] is excellent.

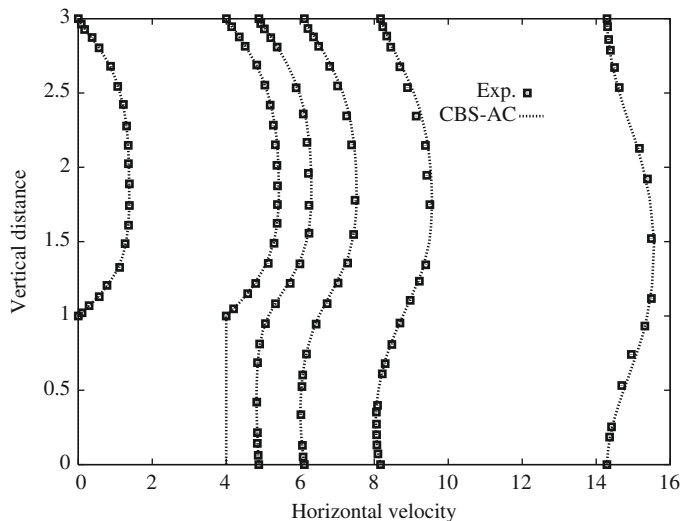
Example 4.3. Steady flow past a sphere

The next problem considered is fully three-dimensional and shows flow past a sphere. The computational domain is a rectangular imaginary box of length $25D$, where D is the diameter of the sphere, with the downstream boundary located $20D$ from the center of the sphere. The four side walls are located at a distance of $5D$ from the center of the sphere. All four confinement walls are assumed to be slip walls with normal velocity equal to zero. The inlet velocity is assumed to be uniform and the no-slip condition prevails on the sphere surface. This problem is solved using the fully explicit form of the CBS scheme.

For this problem, an unstructured grid containing 953,025 tetrahedral elements has been used. This mesh is generated using the mesh generator developed in Swansea [11–14]. Figure 4.11a shows a portion of the surface mesh and Fig. 4.11b shows a

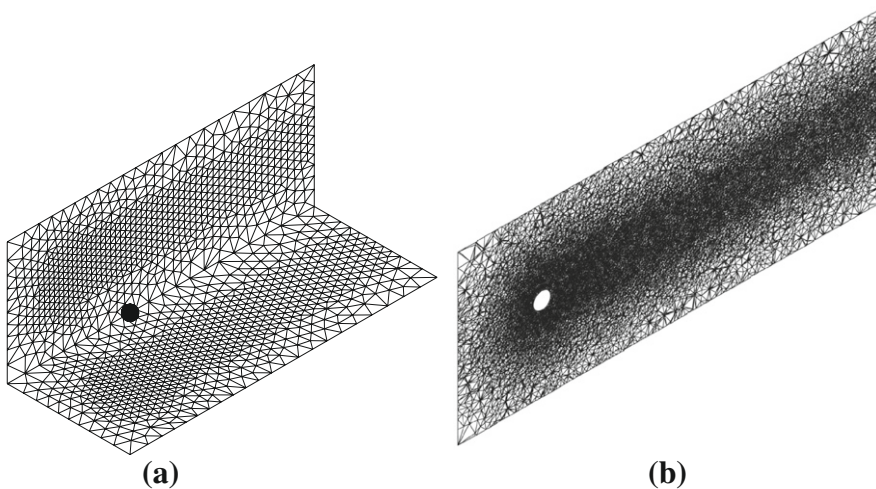
**FIGURE 4.9**

Incompressible flow past a backward facing step: (a) unstructured mesh; (b) u_1 velocity contours; (c) pressure contours ($Re = 229$).

**FIGURE 4.10**

Incompressible flow past a backward facing step. Comparison between experimental [10] and numerical data, $Re = 229$.

sectional view. The mesh is refined close to the sphere surface and in the rear where recirculation is expected. Figure 4.12 shows the contours of the u_1 component of the velocity and the pressures computed at Reynolds numbers of 100 and 200. The coefficient of pressure, C_p , values on the surface along the flow axis are shown in

**FIGURE 4.11**

Incompressible flow past a sphere: (a) unstructured mesh; (b) unstructured mesh, cross section.

Fig. 4.13. The nondimensional C_p is calculated as

$$C_p = 2(p - p_{ref}) \quad (4.10)$$

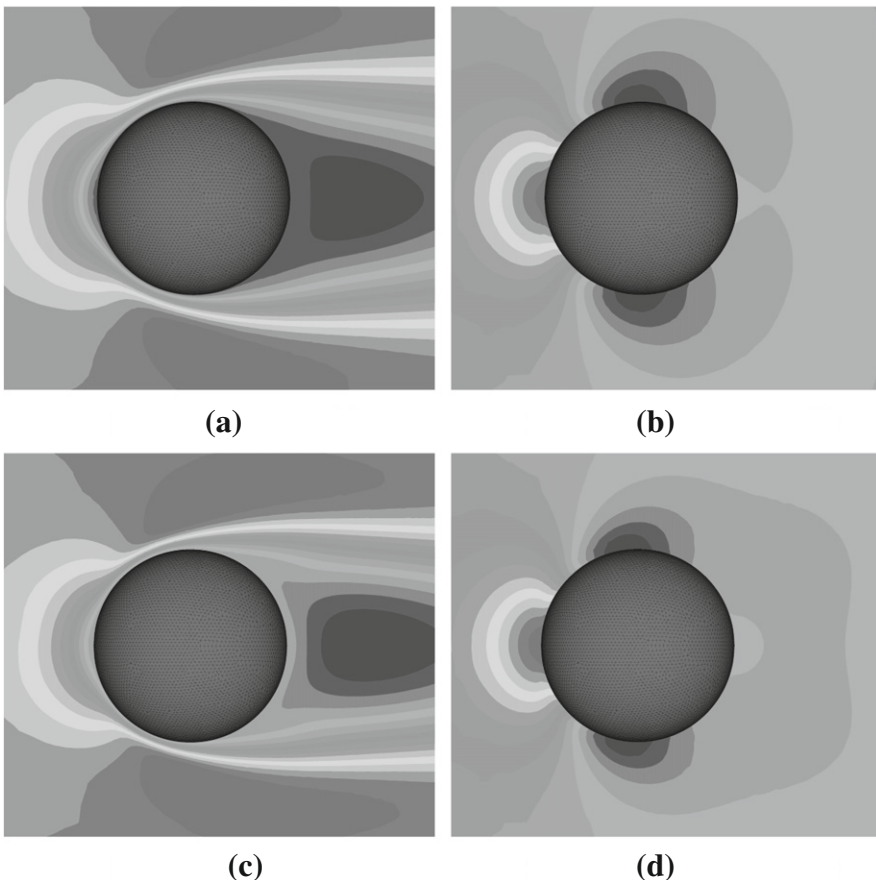
Note that the results used for comparison were generated using very fine structured meshes [15, 16]. It should also be noted that all the results differ from each other close to any separation zone.

Example 4.4. Transient flow past a circular cylinder

This is a popular test case for validating the transient part of numerical schemes. Many other problems of interest can also be solved for transient accuracy but in this section only flow over a single circular cylinder is considered.

Problem definition is standard. The inlet flow is uniform and the cylinder is placed at the centerline between two slip walls. The distances from the inlet and slip walls to the center of the cylinder are $4D$, where D is the diameter of the cylinder. The total length of the domain is $16D$. A no-slip condition is applied on the cylinder surface. The initial values of horizontal velocity were assumed to be unity and the vertical component of velocity was assumed to be zero all over the domain.

Figure 4.14 shows the mesh used in two dimensions and the solution obtained. As seen the mesh close to the cylinder is very fine in order to capture the boundary layer and separation. **Figure 4.14b** and c show the time history of the vertical velocity component at the mid-exit point and the drag coefficient. Both the histories are in good agreement with many reported results.

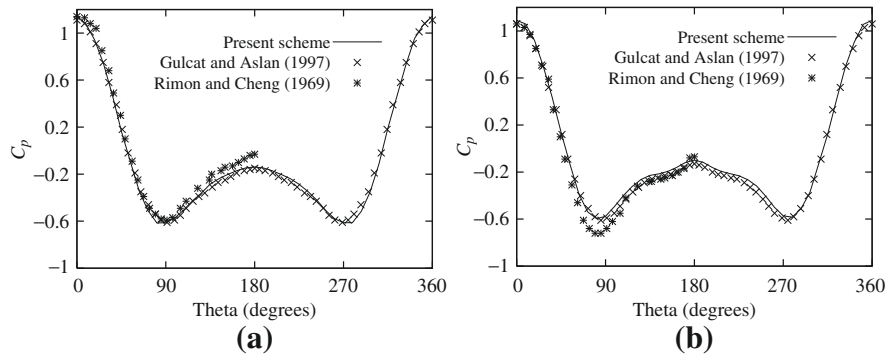
**FIGURE 4.12**

Incompressible flow past sphere: (a) u_1 contours, $Re = 100$; (b) pressure contours, $Re = 100$; (c) u_1 contours, $Re = 200$; pressure contours, $Re = 200$.

4.2.3 Quasi-implicit solution

We have already remarked in [Chapter 3](#) that the reduction of the explicit time step due to viscosity can be very inconvenient and may require a larger number of time steps. The example of the cavity is precisely in that category and at higher Reynolds numbers the reader will certainly note a very large number of time steps which have to be performed before results become reasonably steady. In quasi-implicit form, the viscous terms of the momentum equations are treated implicitly [18]. Here the time step is governed only by the relation given in [Eq. \(4.7\)](#).

It is also possible to incorporate dual time stepping into the quasi-implicit method (or semi-implicit method) as discussed in [Chapter 3](#). Such a formulation allows us

**FIGURE 4.13**

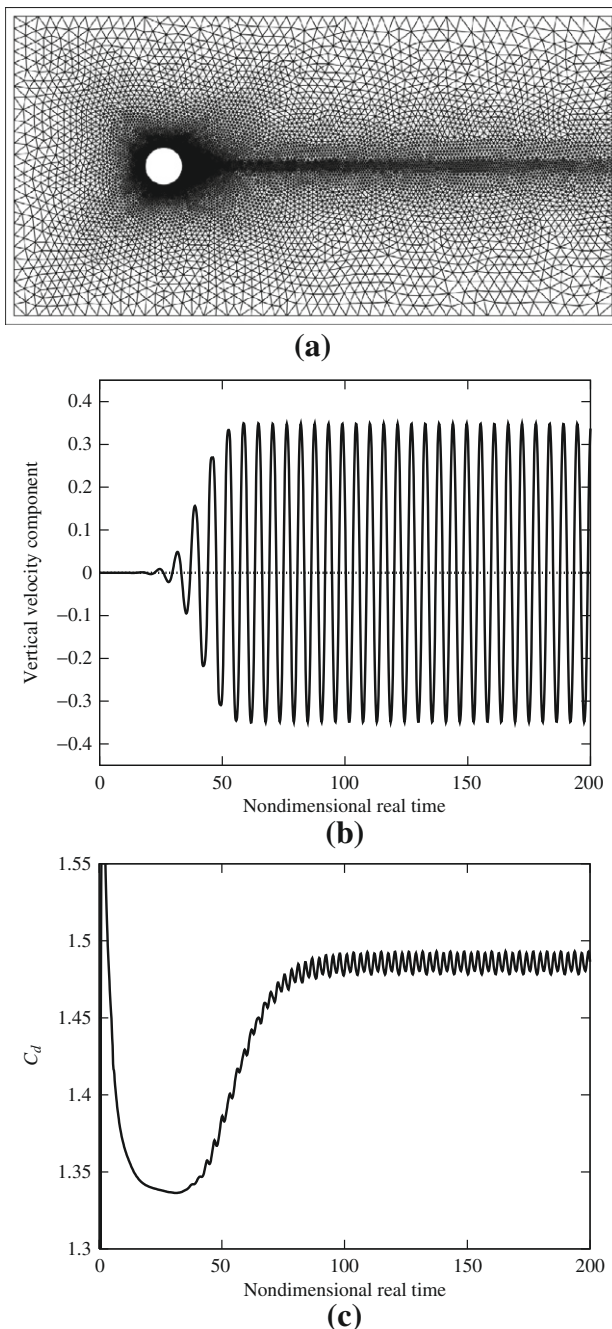
Incompressible flow past a sphere. Coefficient of pressure distribution on the surface along the flow direction [15–17]: (a) $\text{Re} = 100$; (b) $\text{Re} = 200$.

to use a locally defined pseudo time step to accelerate the solution to instantaneous or final steady state. Calculations show that a substantial savings in computational time can be achieved using such a formulation for both steady and unsteady problems [19]. To demonstrate this, steady flow in the lid-driven cavity is reconsidered here at a Reynolds number of 1000 [5]. The nonuniform structured mesh employed consists of 28,800 linear triangular elements and 14,641 nodes. The mesh is refined in the vicinity of the boundaries, with an area ratio of 365 between the largest and smallest elements. Figure 4.15 presents the horizontal and vertical velocity distributions along mid-vertical and mid-horizontal cuts, respectively. As seen, the results from both the global and local time stepping schemes are in excellent agreement with each other and with those predicted by Ghia et al. [5].

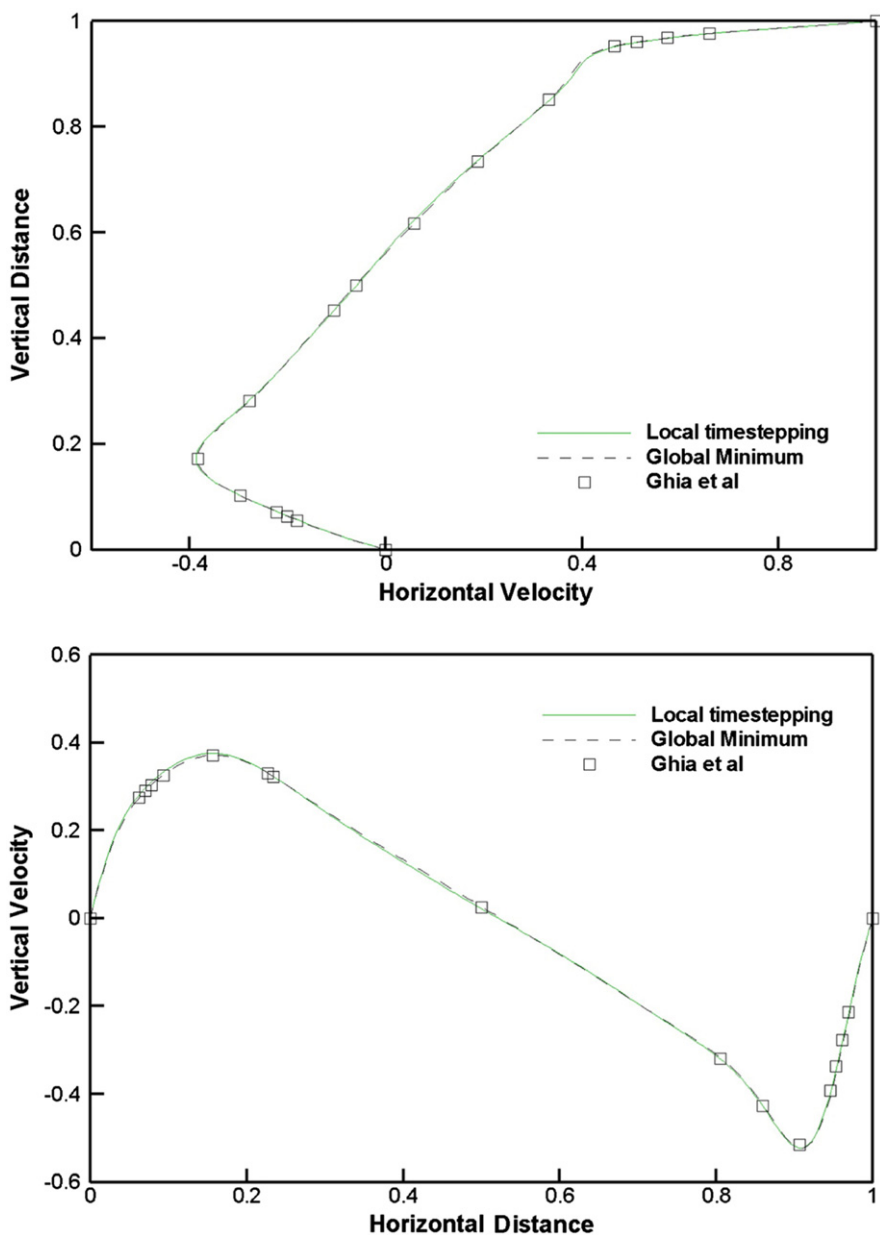
From the quantitative results in Fig. 4.15 and Table 4.1, it is clear that the local time-stepping approach provides almost identical results to that of the global time-stepping approach. However, the computational cost is significantly different as presented in Table 4.2. A single core of an Intel Nehalem quad-core (3 GHz) CPU was employed. From the table, the local time stepping-based quasi-implicit scheme requires only 18.5% of the computational cost. Thus, the speed-up advantage of the local time stepping is clear in this case. Such a reduction in computational time is also possible for transient problems [19].

4.3 Adaptive mesh refinement

We have discussed the matter of adaptive refinement in Chapters 15 and 16 of Ref. [1] in some detail. In that reference generally an attempt is made to keep energy norm error constant within all elements. The same procedures concerning the energy norm error can be extended of course to viscous flow especially when this is relatively slow and the problem is nearly elliptic. However, the energy norm has little significance

**FIGURE 4.14**

Transient flow past a circular cylinder, $Re = 100$: (a) unstructured mesh; (b) vertical velocity fluctuation at the exit mid-point; (c) drag history.

**FIGURE 4.15**

Lid-driven cavity. Horizontal and vertical velocity distributions along the centerline cross-sections, $Re = 1000$.

Table 4.1 Lid-Driven Cavity Problem: Predicted Vortex Locations and Comparison with the Simulation of Ghia et al. [5], Re = 1000

Location	Primary Vortex		Bottom Right (First Vortex)	
	x	y	x	y
Ghia et al.	0.531	0.562	0.859	0.109
Global minimum	0.532	0.566	0.865	0.112
Local time stepping	0.531	0.566	0.862	0.114

Table 4.2 Lid-Driven Cavity: Computational Cost, Re = 1000

	Run Time (s)
Global minimum	7532.1
Local time stepping	1396.2

at high speeds and here we revert to other considerations which simply give an *error indicator* rather than an error estimator. Two procedures are available and will be used in this chapter as well as later when dealing with compressible flows. References [11, 12, 14, 20–82] list some of the many contributions to the field of adaptive procedures and mesh generation in fluid dynamics.

4.3.1 Second gradient (curvature) based refinement

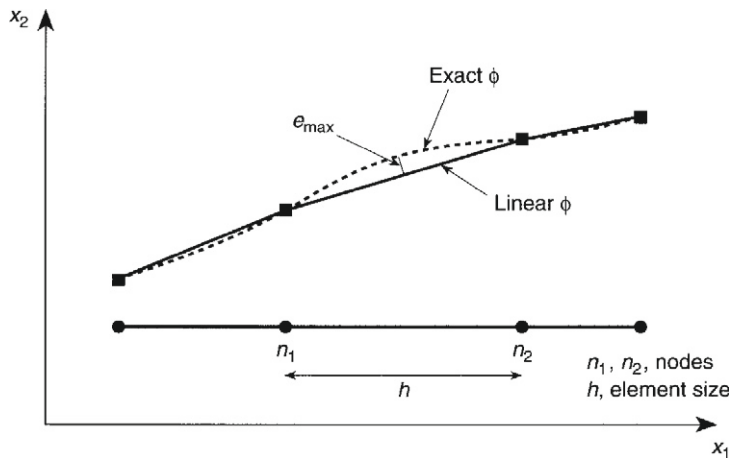
Here the meaning of error analysis is somewhat different from that of the energy norm and we follow an approach where the error value is constant in each element. In what follows we shall consider first-order (linear) elements and the so-called h refinement process in which increased accuracy is achieved by variation of element size. The p refinement in which the order of the element polynomial expression is changed is of course possible. Many studies are available on hp refinements where both h and p refinements are carried out simultaneously. This has been widely studied by Oden et al. [27, 28, 43, 44] but we believe that such refinements impose many limitations on mesh generation and solution procedures and as most fluid mechanics problems involve an explicit time marching algorithm, the higher-order elements are not popular.

The determination of error indicators in linear elements is achieved by consideration of the so-called *interpolation error*. Thus if we take a one-dimensional element of length h and a scalar function ϕ , it is clear that the error in ϕ is of order $O(h^2)$ and that it can be written as (see Ref. [21] for details)

$$e = \phi - \phi^h = ch^2 \frac{d^2\phi}{dx^2} \approx ch^2 \frac{d^2\phi^h}{dx^2} \quad (4.11)$$

where ϕ^h is the finite element solution and c is a constant.

If, for instance, we further assume that $\phi = \phi^h$ at the nodes, i.e., that the nodal error is zero, then e represents the values on a parabola with a curvature of $d^2\phi^h/dx^2$. This

**FIGURE 4.16**

Interpolation error in a one-dimensional problem with linear shape functions.

allows c , the unknown constant, to be determined, giving for instance the maximum interpolation error as (see Fig. 4.16)

$$e_{\max} = \frac{1}{8}h^2 \frac{d^2\phi^h}{dx^2} \quad (4.12)$$

or an RMS departure error as

$$e_{\text{RMS}} = \frac{1}{\sqrt{120}}h^2 \frac{d^2\phi^h}{dx^2} \quad (4.13)$$

In deducing Eqs. (4.12) and (4.13), we have assumed that the nodal values of the function ϕ are exact. As is shown in Ref. [1] this is true only for some types of interpolating functions and equations. However the nodal values are always more accurate than those noted elsewhere and it would be sensible even in one-dimensional problems to strive for equal distribution of such errors. This would mean that we would now seek an element subdivision in which

$$h^2 \frac{d^2\phi^h}{dx^2} = C \quad (4.14)$$

To appreciate the value of the arbitrary constant C occurring in Eq. (4.14) we can interpret this as giving a permissible value of the limiting interpolation error and simply insisting that

$$h^2 \frac{d^2\phi^h}{dx^2} \leq e_p \quad (4.15)$$

where $e_p = C$ is the user-specified error limit.

If we consider the shape functions of ϕ to be linear then of course second derivatives are difficult quantities to determine. These are clearly zero inside every element and infinity at the element nodes in the one-dimensional case or element interfaces in two or three dimensions. Some averaging process has therefore to be used to determine the curvatures from nodally computed values. Before discussing, however, the procedures used for this, we must note the situation which will occur in two or three dimensions.

The extension to two or three dimensions is of course necessary for practical engineering problems. In two and three dimensions the second derivatives (or curvatures) are tensor valued and given as

$$\frac{\partial^2 \phi}{\partial x_i \partial x_j} \quad (4.16)$$

and such definitions require the determination of the *principal values* and directions. These principal directions are necessary for element elongation, which is explained in the following section.

The determination of the curvatures (or second derivatives) of ϕ^h needs of course some elaboration. With linear elements (e.g., simple triangles or tetrahedra) the curvatures of ϕ^h which are interpolated as

$$\phi^h = \mathbf{N}\tilde{\phi} \quad (4.17)$$

are zero within the elements and become infinity at element boundaries. There are two convenient methods available for the determination of curvatures of the approximate solution which are accurate and effective. Both of these follow some of the matter discussed in Chapter 15 of Ref. [1] and are concerned with recovery. We shall describe them separately.

4.3.2 Local patch interpolation: Superconvergent values

In the first method we simply assume that the values of the function such as pressure or velocity converge at a rate which is one order higher at nodes than that achieved at other points of the element. If indeed such values are more accurate it is natural that they should be used for interpreting the curvatures and the gradients. Here the simplest way is to assume that a second-order polynomial is used to interpolate the nodal values in an element patch which uses linear elements. Such a polynomial can be applied in a least-squares manner to fit the values at all nodal points occurring within a patch which assembles the approximation at a particular node. For triangles this rule requires at least five elements that are assembled in a patch and this is a matter easily achieved. The procedure of determining such least squares is given fully in Chapter 15 of Ref. [1] and will not be discussed here. However once a polynomial distribution of say ϕ is available then immediately the second derivatives of that function can be calculated at any point, the most convenient one being of course the point referring to the node which we require.

On occasion, as we shall see in other processes of refinement, it is not the curvature which is required but the gradient of the function. Again the maximum value of the gradient, for instance of ϕ , can easily be determined at any point of the patch and in particular at the nodes.

4.3.3 Estimation of second derivatives at nodes

In this method we assume that the second derivative is interpolated in exactly the same way as the main function and write the approximation as

$$\left(\frac{\partial^2 \phi}{\partial x_i \partial x_j} \right)^h = \mathbf{N} \overline{\left(\frac{\partial^2 \phi}{\partial x_i \partial x_j} \right)^*} \quad (4.18)$$

This approximation is made to be a weighted residual approximation to the actual distribution of curvatures, i.e.,

$$\int_{\Omega} \mathbf{N}^T \left[\mathbf{N} \overline{\left(\frac{\partial^2 \phi}{\partial x_i \partial x_j} \right)^*} - \frac{\partial^2 \phi^h}{\partial x_i \partial x_j} \right] d\Omega = 0 \quad (4.19)$$

and integrating by parts to give

$$\overline{\left(\frac{\partial^2 \phi}{\partial x_i \partial x_j} \right)^*} = \mathbf{M}^{-1} \left(\int_{\Omega} \mathbf{N}^T \frac{\partial^2 \phi^h}{\partial x_i \partial x_j} \right) d\Omega = -\mathbf{M}^{-1} \left(\int_{\Omega} \frac{\partial \mathbf{N}^T}{\partial x_i} \frac{\partial \mathbf{N}}{\partial x_j} d\Omega \right) \tilde{\boldsymbol{\phi}} \quad (4.20)$$

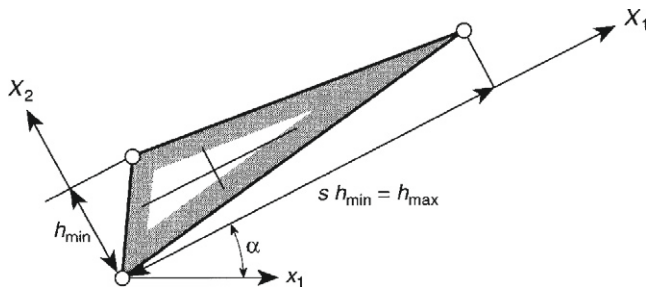
where \mathbf{M} is the mass matrix given by

$$\mathbf{M} = \int_{\Omega} \mathbf{N}^T \mathbf{N} d\Omega \quad (4.21)$$

which of course can be “lumped.”

4.3.4 Element elongation

Elongated elements are frequently introduced to deal with “one-dimensional” phenomena such as shocks, boundary layers, etc. The first paper dealing with such elongation was presented as early as 1987 by Peraire et al. [21]. But the possible elongation was limited by practical considerations if a general mesh of triangles was to be used. An alternative to this is to introduce a locally structured mesh in shocks and boundary layers which connects to the completely unstructured triangles. This idea has been extensively used by Hassan et al. [11, 47, 48], Zienkiewicz and Wu [42], and Marchant et al [56] in the compressible flow context. In both procedures it is necessary to establish the desired elongation of elements. Obviously in completely parallel flow phenomena no limit on elongation exists but in a general field the elongation ratio defining the maximum to minimum size of the element can be derived by considering curvatures of the contours. Thus the local error is proportional to the curvature and making h^2 times the curvature equal to a constant, we immediately derive the ratio h_{\max}/h_{\min} .

**FIGURE 4.17**

Element elongation δ and minimum and maximum element sizes.

In Fig. 4.17, X_1 and X_2 are the directions of the minimum and maximum principal values of the curvatures. Thus for an equal distribution of the interpolation error we can write for each node²

$$h_{\min}^2 \left| \frac{\partial^2 \phi}{\partial X_2^2} \right| = h_{\max}^2 \left| \frac{\partial^2 \phi}{\partial X_1^2} \right| = C \quad (4.22)$$

which gives us the stretching ratio s as

$$s = \frac{h_{\max}}{h_{\min}} = \sqrt{\frac{\left| \frac{\partial^2 \phi}{\partial X_2^2} \right|}{\left| \frac{\partial^2 \phi}{\partial X_1^2} \right|}} \quad (4.23)$$

With the relations given above, we can formulate the following steps to adaptively refine a mesh:

1. Find the solution using an initial coarse mesh.
2. Select a suitable representative scalar variable and calculate the local maximum and minimum curvatures and directions of these at all nodes.
3. Calculate the new element sizes at all nodes from the maximum and minimum curvatures using the relation in Eq. (4.22).
4. Calculate the stretching ratio from the ratio of the calculated maximum to minimum element sizes [Eq. (4.23)]. If this is very high, limit it by a maximum allowable value.
5. Remesh the whole domain based on the new element size, stretching ratios, and the direction of stretching.

²Principal curvatures and directions can be found in a manner analogous to that of the determination of principal stresses and their directions. Procedures are described in standard engineering texts.

To use the above procedure, an efficient unstructured mesh generator is essential. We normally use the advancing front technique operating on the background mesh principle [21] in most of the examples presented here.³ The information from the previous solution in the form of local mesh sizes, stretching ratio, and stretching direction are stored in the previous mesh and this mesh is used as a background mesh for the new mesh.

In the above steps of anisotropic mesh generation, to avoid very small and large elements (especially in compressible flows), the minimum and maximum allowable sizes of the elements are given as inputs. The maximum allowable stretching ratio is also supplied to the code to avoid bad elements in the vicinity of discontinuities. It is generally useful to know the minimum element size used in a mesh as many flow solvers are conditionally stable. In such solvers the time step limitation depends very much on the element size.

The procedure just described for an elongated element can of course be applied for the generation of isotropic meshes simply by taking the maximum curvature at every point.

The matter to which we have not yet referred is that of suitably choosing the variable ϕ to which we will wish to assign the error. We shall come back to this matter later but it is clear that this has to be a well-representative quantity available from the choice of velocities, pressures, temperature, etc.

4.3.5 First derivative (gradient) based refinement

The nature of the fluid flow problems is elliptic in the vicinity of the boundaries often forming so-called viscous boundary layers though some distance from the boundaries the equations become almost hyperbolic. For such hyperbolic problems it is possible to express the propagation type error in terms of the gradient of the solution in the domain. In such cases the error can be considered as

$$h \frac{\partial \phi}{\partial n} = C \quad (4.24)$$

where n is the direction of maximum gradient and h is the element size (minimum size) in the same direction. The above expression can be used to determine the minimum element size at all nodes or other points of consideration in exactly the same manner as was done when using the curvature. However the question of stretching is less clear. At every point a maximum element size should be determined. One way of doing this is of course to return to the curvatures and find the curvature ratios. Another procedure to determine the maximum element size is described by Zienkiewicz and Wu [42]. In this the curvature of the streamlines is considered and h_{\max} is calculated as

$$h_{\max} \leq \delta R \quad (4.25)$$

³Another successful unstructured mesh generator is based on Delaunay triangulation. The reader can obtain more information by consulting Refs. [12, 14, 51–53, 74, 76, 79–81].

where R is the radius of curvature of the streamline and δ is a constant that varies between 0 and 1. Immediately the ratio between the maximum and minimum element size gives the stretching ratio.

4.3.6 Choice of variables

In both methods of mesh refinement, i.e., those following curvatures and those following gradients, a particular scalar variable needs to be chosen to define the mesh. The simplest procedure is to consider only one of the many variables and here the one which is efficient is simply the absolute value of the velocity vector, i.e., $|\mathbf{u}|$. Such a velocity is convenient both for problems of incompressible flow and, as we shall see later, for problems of compressible flow where local refinement is even more important than here. (Very often in compressible flows the Mach number, which in a sense measures the same quantity, has been used.)

Of course other variables can be chosen or any combination of variables such as velocities, pressures, temperatures, etc., can be used. Certainly in this chapter the absolute velocity is the most reasonable criterion. Some authors have considered using each of the problem variables to generate a new mesh [45, 52, 53, 60, 83]. However this is rather expensive and we believe velocity alone can give accurate results in most cases.

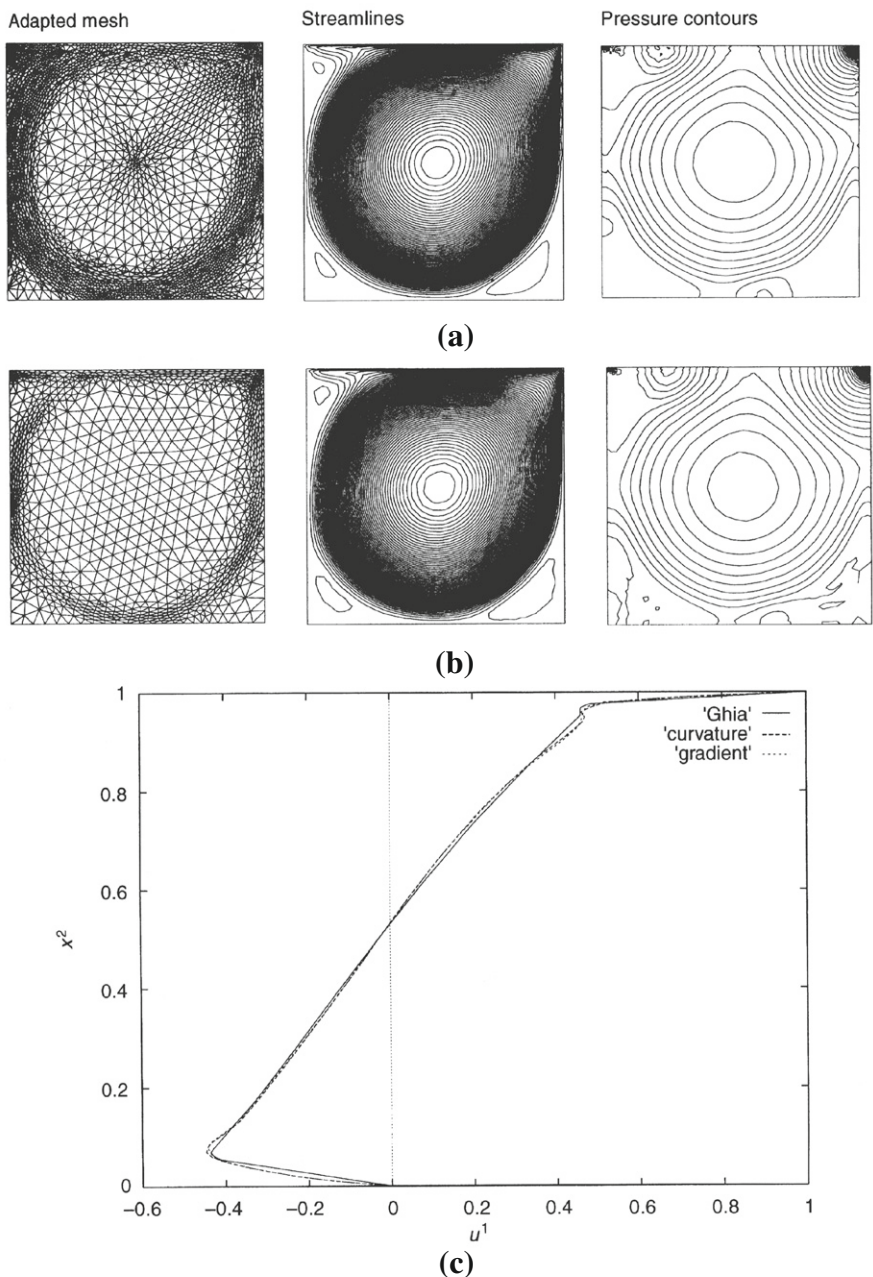
4.3.7 An example

Here we show an example of an incompressible flow problem solved using the above-mentioned adaptive mesh generation procedures. In the first problem of driven flow in a cavity which we have previously examined is again used. We use an initial uniform mesh with 481 nodes and 880 elements. Final meshes and solutions obtained by both curvature- and gradient-based procedures are shown in Fig. 4.18. In general the curvature-based procedure gives a wide band of refined elements along the circulation path (Fig. 4.18a). However, the number of refined elements along the circulation path is smaller when the gradient-based refinement is used (Fig. 4.18b). Both the meshes give excellent comparison with the benchmark solution of Ghia et al. [5] (Fig. 4.18c).

In the adaptive solutions shown here we have not used any absolute value of the desired error norm as the definition of a suitable norm presents certain difficulties, though of course the use of an energy norm in the manner suggested in Ref. [1] could be adopted. We shall use such an error requirement in some later problems.

4.4 Adaptive mesh generation for transient problems

In the preceding sections we have indicated various adaptive methods using complete mesh regeneration with error indicators of the interpolation kind. Obviously other methods of mesh refinement can be used (mesh enrichment or r refinement) and other procedures of error estimation can be employed if the problem is nearly elliptic. One such study in which the energy norm is quite effectively used is reported by Wu

**FIGURE 4.18**

Lid-driven cavity, $Re = 5000$. Adapted meshes using curvature- and gradient-based refinements and solutions: (a) curvature-based procedure (nodes: 2389, elements: 4599); (b) gradient-based procedure (nodes: 1034, elements: 1962); (c) comparison of velocity at mid-vertical plane.

et al. [32]. In that study the full transient behavior of the *Von Karman* vortex street behind a cylinder was considered and the results are presented in Fig. 4.19.

In this problem, the mesh is regenerated at fixed time intervals using the energy norm error and the methodologies largely described in Chapter 16 of Ref. [1].

Similar procedures have been used by others and the reader can refer to these works [33,34].

4.5 Slow flows: Mixed and penalty formulations

4.5.1 Analogy with incompressible elasticity

Slow, viscous incompressible flow represents the extreme situation at the other end of the scale from the inviscid problem of Section 1.3. Here all dynamic (acceleration) forces are, *a priori*, neglected and Eqs. (4.1) and (4.2) reduce, in indicial form, to

$$\frac{\partial u_i}{\partial x_i} \equiv \dot{\varepsilon}_v = 0 \quad (4.26)$$

and

$$\frac{\partial \tau_{ij}}{\partial x_j} - \frac{\partial p}{\partial x_i} + \rho g_i = 0 \quad (4.27)$$

The above are completed of course by the constitutive relation

$$\tau_{ij} = \mu \left(\frac{\partial u_i}{\partial x_j} + \frac{\partial u_j}{\partial x_i} \right) \quad (4.28)$$

which is identical to the problem of incompressible elasticity in which we replace

- (a) The displacements by velocities
- (b) The shear modulus G by the viscosity μ
- (c) The mean stress by negative pressure

4.5.2 Mixed and penalty discretization

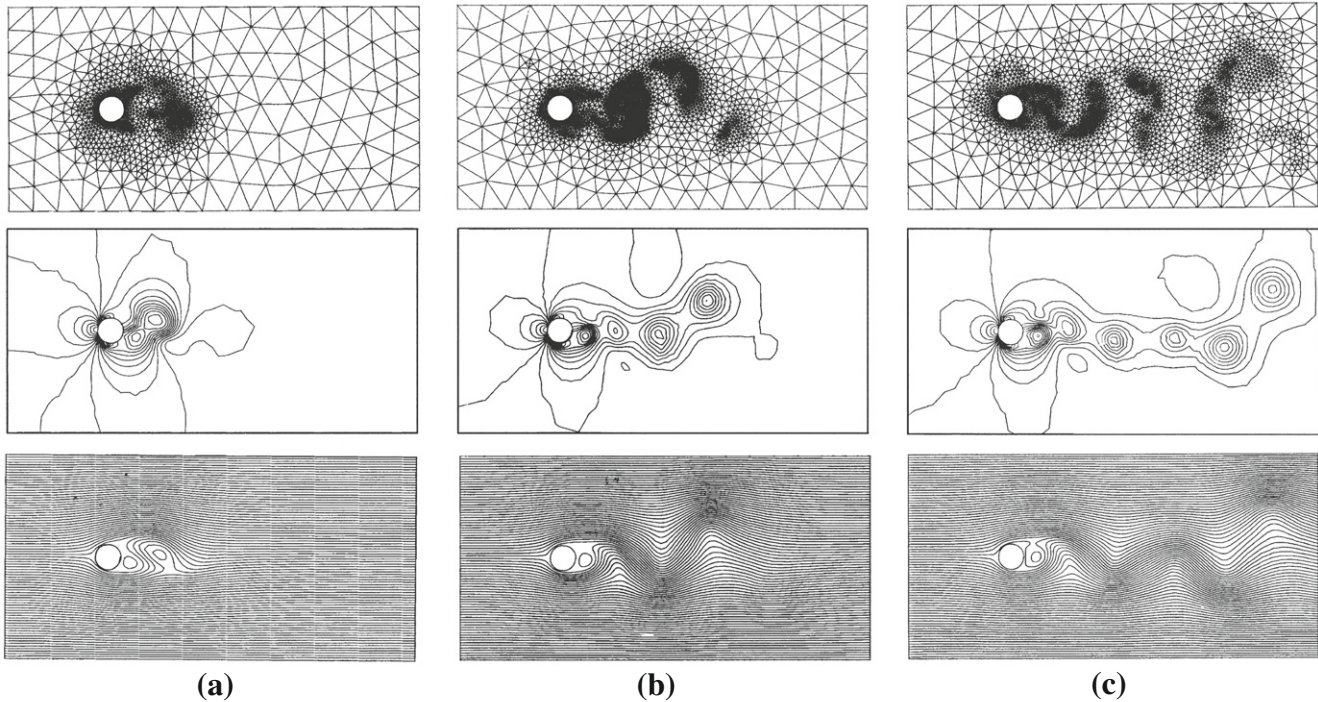
The discretization can be started from the *mixed form* with independent approximations of \mathbf{u} and p , i.e.,

$$\mathbf{u} = \mathbf{N}_u \tilde{\mathbf{u}} \quad p = \mathbf{N}_p \tilde{\mathbf{p}} \quad (4.29)$$

or by a penalty form in which Eq. (4.26) is augmented by p/γ where γ is a large penalty parameter

$$\mathbf{m}^T \mathcal{S} \mathbf{u} + \frac{p}{\gamma} = 0 \quad (4.30)$$

When suitable discontinuous \mathbf{N}_p are used, penalty terms computed using reduced integration are equivalent to the mixed form [84] (see Chapter 9 of Ref. [1] for details).

**FIGURE 4.19**

Transient incompressible flow around a cylinder at $Re = 250$. Adaptively refined mesh. Pressure contours and streamlines at various times after initiation of “vortex shedding”: (a) $t = 6$ s; (b) $t = 11.5$ s; (c) $t = 16.5$ s.

The use of penalty forms in fluid mechanics was introduced early in the 1970s [85–87] and is fully discussed elsewhere [88–90]. As computationally it is advantageous to use the mixed form and introduce the penalty parameter only to eliminate the $\tilde{\mathbf{p}}$ values at the element levels, we shall presume such penalization to be done after the mixed discretization.

The discretized equations will always be of the form

$$\begin{bmatrix} \mathbf{K} & -\mathbf{G} \\ -\mathbf{G}^T & -\mathbf{V}/\gamma \end{bmatrix} \begin{Bmatrix} \tilde{\mathbf{u}} \\ \tilde{\mathbf{p}} \end{Bmatrix} = \begin{Bmatrix} \bar{\mathbf{f}} \\ \mathbf{0} \end{Bmatrix} \quad (4.31)$$

in which

$$\begin{aligned} \mathbf{K} &= \int_{\Omega} \mathbf{B}^T \mu \mathbf{I}_0 \mathbf{B} d\Omega \quad \text{where } \mathbf{B} \equiv \mathcal{S} \mathbf{N}_u \\ \mathbf{G} &= \int_{\Omega} \mathbf{B}^T \mathbf{m} \mathbf{N}_p d\Omega, \quad \mathbf{V} = \int_{\Omega} \mathbf{N}_p^T \mathbf{N}_p d\Omega \\ \bar{\mathbf{f}} &= \int_{\Omega} \mathbf{N}_u^T \rho \mathbf{g} d\Omega + \int_{\Gamma_t} \mathbf{N}_u^T \bar{\mathbf{t}} d\Gamma \end{aligned} \quad (4.32)$$

and the penalty number, γ , is introduced purely as a numerical convenience. This is taken generally as [88, 90]

$$\gamma = (10^7 - 10^8) \mu$$

There is little more to be said about the solution procedures for creeping incompressible flow with constant viscosity. The range of applicability is of course limited to low velocities of flow or high viscosity fluids such as oil, blood in biomechanics applications, etc. It is, however, important to recall here that the mixed form allows only certain combinations of \mathbf{N}_u and \mathbf{N}_p interpolations to be used without violating the convergence conditions. This is discussed in detail in Chapter 10 of Ref. [1], but for completeness Fig. 4.20 lists some of the available elements together with their asymptotic convergence rates [91]. Many other elements useful in fluid mechanics are documented elsewhere [92–94], but those of proven performance are given in the table.

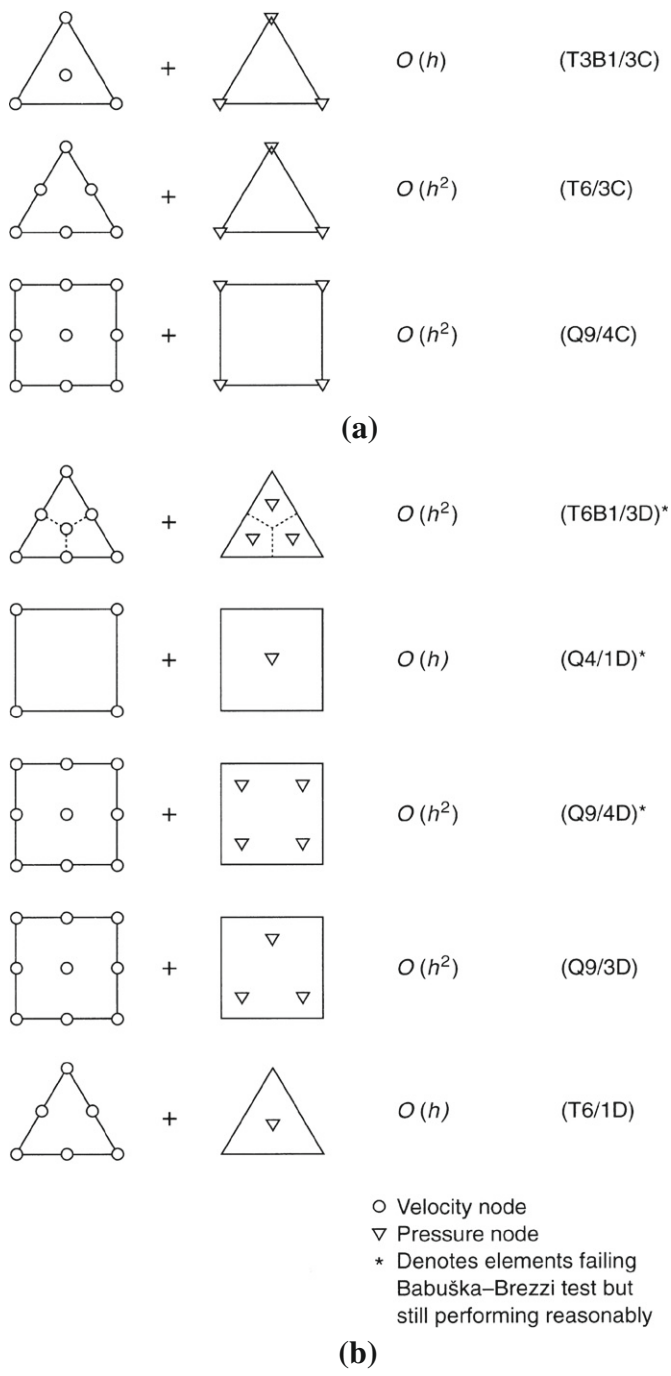
It is of general interest to note that frequently elements with C_0 continuous pressure interpolations are used in fluid mechanics and indeed that their performance is generally superior to those with discontinuous pressure interpolation on a given mesh, even though the cost of solution is marginally greater.

It is important to note that the recommendations concerning the element types for the Stokes problem carry over unchanged to situations in which dynamic terms are of importance.

The fairly obvious extension of the use of incompressible elastic codes to Stokes flow is undoubtedly the reason why the first finite element solutions of fluid mechanics were applied in this area.

4.6 Concluding remarks

The incompressible Newtonian fluid dynamics has been discussed in this chapter. Several more two- and three-dimensional problems can be found in recent publica-

**FIGURE 4.20**

Some useful velocity-pressure interpolations and their asymptotic, energy norm convergence rates: (a) continuous p interpolation; (b) discontinuous p interpolation.

tions on the CBS scheme. In addition to covering several benchmark problems of incompressible flows, we also have discussed several adaptive procedures for fluid dynamics problems. The chapter finally concludes by briefly describing the penalty methods.

References

- [1] O.C. Zienkiewicz, R.L. Taylor, J.Z. Zhu, *The Finite Element Method: Its Basis and Fundamentals*, seventh ed., Elsevier, Oxford, 2013.
- [2] P. Nithiarasu, An efficient artificial compressibility (AC) scheme based on the characteristic based split (CBS) method for incompressible flows, *Int. J. Numer. Methods Eng.* 56 (2003) 1815–1845.
- [3] P. Nithiarasu, J.S. Mathur, N.P. Weatherill, K. Morgan, Three-dimensional incompressible flow calculations using the characteristic based split (CBS) scheme, *Int. J. Numer. Methods Fluids* 44 (2004) 1207–1229.
- [4] R. Codina, M. Vázquez, O.C. Zienkiewicz, General algorithm for compressible and incompressible flows, Part III – a semi-implicit form, *Int. J. Numer. Methods Fluids* 27 (1998) 13–32.
- [5] U. Ghia, K.N. Ghia, C.T. Shin, High-resolution for incompressible flow using the Navier-Stokes equations and multigrid method, *J. Comput. Phys.* 48 (1982) 387–411.
- [6] P.N. Shankar, M.D. Deshpande, Fluid mechanics in the driven cavity, *Annu. Rev. Fluid Mech.* 32 (2000) 93–136.
- [7] A. Yeckel, J.W. Smith, J.J. Derby, Parallel finite element calculation of flow in a three-dimensional lid-driven cavity using the CM-5 and T3D, *Int. J. Numer. Methods Fluids* 24 (1997) 1449–1461.
- [8] L.Q. Tang, T.W. Cheng, T.T.H. Tsang, Transient solutions for 3-dimensional lid-driven cavity flows by a least-squares finite element method, *Int. J. Numer. Methods Fluids* 21 (1995) 413–432.
- [9] J. Kim, P. Moin, Application of a fractional step method to incompressible Navier-Stokes equations, *J. Comput. Phys.* 59 (1985) 308–323.
- [10] M.K. Denham, M.A. Patrik, Laminar flow over a downstream-facing step in a two-dimensional flow channel, *Trans. Inst. Chem. Eng.* 52 (1974) 361–367.
- [11] O. Hassan, E.J. Probert, K. Morgan, J. Peraire, Mesh generation and adaptivity for the solution of compressible viscous high speed flows, *Int. J. Numer. Methods Eng.* 38 (1995) 1123–1148.
- [12] N.P. Weatherill, O. Hassan, Efficient 3-dimensional Delaunay triangulation with automatic point generation and imposed boundary constraints, *Int. J. Numer. Methods Eng.* 37 (1994) 2005–2039.
- [13] K. Morgan, J. Peraire, Unstructured grid finite element methods for fluid mechanics, *Rep. Prog. Phys.* 61 (1998) 569–638.

- [14] N.P. Weatherill, O. Hassan, D.L. Marcum, Compressible flow field solutions with unstructured grids generated by Delaunay triangulation, *J. AIAA* 33 (1995) 1196–1204.
- [15] Ü. Gülcat, A.R. Aslan, Accurate 3D viscous incompressible flow calculations with FEM, *Int. J. Numer. Methods Fluids* 25 (1997) 985–1001.
- [16] Y. Rimon, S.I. Cheng, Numerical solution of a uniform flow over a sphere at intermediate reynolds numbers, *Phys. Fluids* 12 (1969) 949–959.
- [17] P. Nithiarasu, N. Massarotti, J.S. Mathur, Forced convection heat transfer from solder balls on a printed circuit board using the characteristic based split (CBS) scheme, *Int. J. Numer. Methods Heat Fluid Flow* 15 (1) (2005) 73–95.
- [18] R. Codina, M. Vázquez, O.C. Zienkiewicz, A fractional step method for the solution of compressible Navier-Stokes equations, in: M. Hafez, K. Oshima (Eds.), *Computational Fluid Dynamics Review*, vol. 1, World Scientific Publishing, 1998, pp. 331–347.
- [19] R.L.T. Bevan, P. Nithiarasu, Accelerating incompressible flow calculations using a quasi-implicit scheme: local and dual time stepping approaches, *Comput. Mech.* 50 (6, SI) (2012) 687–693.
- [20] R. Löhner, K. Morgan, O.C. Zienkiewicz, An adaptive finite element procedure for compressible high speed flows, *Comput. Methods Appl. Mech. Eng.* 51 (1985) 441–465.
- [21] J. Peraire, M. Vahdati, K. Morgan, O.C. Zienkiewicz, Adaptive remeshing for compressible flow computations, *J. Comput. Phys.* 72 (1987) 449–466.
- [22] J.T. Oden, T. Strouboulis, P. Devloo, Adaptive finite element methods for high speed compressible flows, *Int. J. Numer. Methods Eng.* 7 (1987) 1211–1228.
- [23] J. Peraire, K. Morgan, O.C. Zienkiewicz, Convection dominated problems, *Numerical Methods for Compressible Flows – Finite Difference, Element and Volume Techniques*, vol. AMD 78, ASME, New York, 1987.
- [24] O.C. Zienkiewicz, J.Z. Zhu, Y.C. Liu, K. Morgan, J. Peraire, Error estimates and adaptivity. From elasticity to high speed compressible flow, in: J. Whiteman (Ed.), *The Mathematics of Finite Elements and Applications*, vol. VII, Academic Press, London, 1988, pp. 483–512.
- [25] B. Palmerio, A two-dimensional FEM adaptive moving-node method for steady Euler flow simulation, *Comput. Methods Appl. Mech. Eng.* 71 (1988) 315–340.
- [26] R. Löhner, Adaptive remeshing for transient problems, *Comput. Methods Appl. Mech. Eng.* 75 (1989) 195–214.
- [27] L. Demkowicz, J.T. Oden, W. Rachowicz, O. Hardy, Toward a universal $h - p$ adaptive finite element strategy. Part 1: Constrained approximation and data structure, *Comput. Methods Appl. Mech. Eng.* 77 (1989) 79–112.
- [28] J.T. Oden, L. Demkowicz, W. Rachowicz, T.A. Westermann, Toward a universal h-p adaptive finite element strategy. Part 2: A posteriori error estimation, *Comput. Methods Appl. Mech. Eng.* 77 (1989) 113–180.
- [29] O.C. Zienkiewicz, Adaptivity-fluids-localization – the new challenge to computational mechanics, *Tran. Can. Soc. Mech. Eng.* 15 (1991) 137–145.

- [30] E.J. Probert, O. Hassan, K. Morgan, J. Peraire, An adaptive finite element method for transient compressible flows with moving boundaries, *Int. J. Numer. Methods Eng.* 32 (1991) 751–765.
- [31] A. Evans, M.J. Marchant, J. Szmelter, N.P. Weatherill, Adaptivity for compressible flow computations using point embedding on 2-D structured multiblock meshes, *Int. J. Numer. Methods Eng.* 32 (1991) 895–919.
- [32] J. Wu, J.Z. Zhu, J. Szmelter, O.C. Zienkiewicz, Error estimation and adaptivity in Navier-Stokes incompressible flows, *Comput. Mech.* 61 (1991) 30–39.
- [33] J.F. Hetu, D.H. Pelletier, Adaptive remeshing for viscous incompressible flows, *AIAA J.* 30 (1992) 1986–1992.
- [34] J.F. Hetu, D.H. Pelletier, Fast, adaptive finite element scheme for viscous incompressible flows, *AIAA J.* 30 (1992) 2677–2682.
- [35] J. Peraire, J. Peiro, K. Morgan, Adaptive remeshing for 3-dimensional compressible flow computations, *J. Comput. Phys.* 103 (1992) 269–285.
- [36] E.J. Probert, O. Hassan, K. Morgan, J. Peraire, Adaptive explicit and implicit finite element methods for transient thermal analysis, *Int. J. Numer. Methods Eng.* 35 (1992) 655–670.
- [37] J. Szmelter, M.J. Marchant, A. Evans, N.P. Weatherill, 2-dimensional Navier-Stokes equations with adaptivity on structured meshes, *Comput. Methods Appl. Mech. Eng.* 101 (1992) 355–368.
- [38] R. Löhner, J.D. Baum, Adaptive h -refinement on 3D unstructured grid for transient problems, *Int. J. Numer. Methods Fluids* 14 (1992) 1407–1419.
- [39] M.J. Marchant, N.P. Weatherill, Adaptivity techniques for compressible inviscid flows, *Comput. Methods Appl. Mech. Eng.* 106 (1993) 83–106.
- [40] W. Rachowicz, An anisotropic h -type mesh refinement strategy, *Comput. Methods Appl. Mech. Eng.* 109 (1993) 169–181.
- [41] P.A.B. de Sampaio, P.R.M. Lyra, K. Morgan, N.P. Weatherill, Petrov-Galerkin solutions of the incompressible Navier-Stokes equations in primitive variables with adaptive remeshing, *Comput. Methods Appl. Mech. Eng.* 106 (1993) 143–178.
- [42] O.C. Zienkiewicz, J. Wu, Automatic directional refinement in adaptive analysis of compressible flows, *Int. J. Numer. Methods Eng.* 37 (1994) 2189–2219.
- [43] J.T. Oden, W. Wu, M. Ainsworth, An a posteriori error estimate for finite element approximations of the Navier-Stokes equations, *Comput. Methods Appl. Mech. Eng.* 111 (1994) 185–202.
- [44] J.T. Oden, W. Wu, V. Legat, An hp adaptive strategy for finite element approximations of the Navier-Stokes equations, *Int. J. Numer. Methods Fluids* 20 (1995) 831–851.
- [45] M.J. Castro-Díaz, H. Borouchaki, P.L. George, F. Hecht, B. Mohammadi, Anisotropic adaptive mesh generation in two dimensions for CFD, in: *Computational Fluid Dynamics '96*, 1996, pp. 181–186.
- [46] R. Löhner, Mesh adaptation in fluid mechanics, *Eng. Frac. Mech.* 50 (1995) 819–847.

- [47] O. Hassan, K. Morgan, E.J. Probert, J. Peraire, Unstructured tetrahedral mesh generation for three dimensional viscous flows, *Int. J. Numer. Methods Eng.* 39 (1996) 549–567.
- [48] O. Hassan, K. Morgan, E.J. Probert, J. Peraire, Unstructured tetrahedral mesh generation for three dimensional viscous flows, *Int. J. Num. Methods Eng.* 39 (1996) 549–567.
- [49] D.D.D. Yahia, W.G. Habashi, A. Tam, M.G. Vallet, M. Fortin, A directionally adaptive methodology using an edge based error estimate on quadrilateral grids, *Int. J. Numer. Methods Fluids* 23 (1996) 673–690.
- [50] M. Fortin, M.G. Vallet, J. Dompierre, Y. Bourgault, W.G. Habashi, Anisotropic mesh adaption: theory, validation and applications, in: *Computational Fluid Dynamics '96*, 1996, pp. 174–180.
- [51] K.S.V. Kumar, A.V.R. Babu, K.N. Seetharamu, T. Sundararajan, P.A.A. Narayana, A generalized Delaunay triangulation algorithm with adaptive grid size control, *Commun. Appl. Numer. Methods* 13 (1997) 941–948.
- [52] H. Borouchaki, P.L. George, F. Hecht, P. Laug, E. Saltel, Delaunay mesh generation governed by metric specifications. Part I. Algorithms, *Finite Elem. Anal. Des.* 25 (1997) 61–83.
- [53] H. Borouchaki, P.L. George, B. Mohammadi, Delaunay mesh generation governed by metric specifications. Part II. Applications, *Finite Elem. Anal. Des.* 25 (1997) 85–109.
- [54] W. Rachowicz, An anisotropic h -adaptive finite element method for compressible Navier-Stokes equations, *Comput. Methods Appl. Mech. Eng.* 146 (1997) 231–252.
- [55] J. Peraire, K. Morgan, Unstructured mesh generation including directional refinement for aerodynamic flow simulation, *Finite Elem. Anal. Des.* 25 (1997) 343–356.
- [56] M.J. Marchant, N.P. Weatherill, O. Hassan, The adaptation of unstructured grids for transonic viscous flow simulation, *Finite Elem. Anal. Des.* 25 (1997) 199–218.
- [57] H. Borouchaki, F. Hecht, P.J. Frey, Mesh gradation control, *Int. J. Numer. Methods Fluids* 43 (1998) 1143–1165.
- [58] H. Borouchaki, P.J. Frey, Adaptive triangular-quadrilateral mesh generation, *Int. J. Numer. Methods Eng.* 41 (1998) 915–934.
- [59] H. Jin, S. Prudhomme, A posteriori error estimation of steady-state finite element solution of the Navier-Stokes equations by a subdomain residual method, *Comput. Methods Appl. Mech. Eng.* 159 (1998) 19–48.
- [60] P. Nithiarasu, O.C. Zienkiewicz, Adaptive mesh generation procedure for fluid mechanics problems, *Int. J. Numer. Methods Eng.* 47 (2000) 629–662.
- [61] P. Nithiarasu, An adaptive finite element procedure for solidification problems, *Heat Mass Transfer* 36 (3) (2000) 223–229.
- [62] E. De Santiago, K.H. Law, A distributed implementation of an adaptive finite element method for fluid problems, *Comput. Fluids* 74 (2000) 97–119.

- [63] P. Saramito, N. Roquet, An adaptive finite element method for viscoplastic fluid flows in pipes, *Comput. Methods Appl. Mech. Eng.* 190 (40–41) (2001) 5391–5412.
- [64] P. Nithiarasu, An adaptive remeshing technique for laminar natural convection problems, *Heat Mass Transfer* 38 (3) (2002) 243–250.
- [65] N. Roquet, P. Saramito, An adaptive finite element method for Bingham fluid flows around a cylinder, *Comput. Methods Appl. Mech. Eng.* 192 (2003) 3317–3341.
- [66] P. Yue, C. Zhou, J.J. Feng, C.F. Ollivier-Gooch, H.H. Hu, Phase-field simulations of interfacial dynamics in viscoelastic fluids using finite elements with adaptive meshing, *J. Comput. Phys.* 219 (2006) 47–67.
- [67] D.R. Davies, J.H. Davies, O. Hassan, K. Morgan, P. Nithiarasu, Investigations into the applicability of adaptive finite element methods to two-dimensional infinite Prandtl number thermal and thermochemical convection, *Geochem. Geophys. Geosyst.* 8 (2007).
- [68] J. Narski, M. Picasso, Adaptive finite elements with high aspect ratio for dendritic growth of a binary alloy including fluid flow induced by shrinkage, *Comput. Methods Appl. Mech. Eng.* 196 (2007) 3562–3576.
- [69] D.R. Davies, J.H. Davies, O. Hassan, K. Morgan, P. Nithiarasu, Adaptive finite element methods in geodynamics: convection dominated mid-ocean ridge and subduction zone simulations, *Int. J. Numer. Methods Heat Fluid Flow* 18 (7–8) (2008) 1015–1035.
- [70] F. Bengzon, M.G. Larson, Adaptive finite element approximation of multi-physics problems: a fluid-structure interaction model problem, *Int. J. Numer. Methods Eng.* 84 (2010) 1451–1465.
- [71] M.G. Armentano, C. Padra, R. Rodriguez, M. Scheble, An hp finite element adaptive scheme to solve the Laplace model for fluid-solid vibrations, *Comput. Methods Appl. Mech. Eng.* 200 (2011) 178–188.
- [72] X. Garcia, D. Pavlidis, G.J. Gorman, J.L.M.A. Gomes, M.D. Piggott, E. Aristodemou, J. Mindel, J.-P. Latham, C.C. Pain, H. ApSimon, A two-phase adaptive finite element method for solid-fluid coupling in complex geometries, *Int. J. Numer. Methods Fluids* 66 (2011) 82–96.
- [73] P.J. Green, R. Sibson, Computing Dirichlet tessellations in the plane, *Comput. J.* 21 (1978) 168–173.
- [74] D.F. Watson, Computing the n -dimensional Delaunay tessellation with application to Voronoi polytopes, *Comput. J.* 24 (1981) 167–172.
- [75] J.C. Cavendish, D.A. Field, W.H. Frey, An approach to automatic three dimensional finite element mesh generation, *Int. J. Numer. Methods Eng.* 21 (1985) 329–347.
- [76] W.J. Schroeder, M.S. Shephard, A combined octree Delaunay method for fully automatic 3-d mesh generation, *Int. J. Numer. Methods Eng.* 29 (1990) 37–55.
- [77] N.P. Weatherill, Mesh generation for aerospace applications, *Sadhana Acc. Proc. Eng. Sci.* 16 (1991) 1–45.

- [78] N.P. Weatherill, P.R. Eiseman, J. Hause, J.F. Thompson, Numerical Grid Generation in Computational Fluid Dynamics and Related Fields, Pineridge Press, Swansea, 1994.
- [79] G. Subramanian, V.V.S. Raveendra, M.G. Kamath, Robust boundary triangulation and Delaunay triangulation of arbitrary planar domains, *Int. J. Numer. Methods Eng.* 37 (1994) 1779–1789.
- [80] R.W. Lewis, Y. Zhang, A.S. Usmani, Aspects of adaptive mesh generation based on domain decomposition and Delaunay triangulation, *Finite Elem. Anal. Des.* 20 (1995) 47–70.
- [81] H. Borouchaki, P.L. George, Aspects of 2-D Delaunay mesh generation, *Int. J. Numer. Methods Eng.* 40 (1997) 1957–1975.
- [82] J.F. Thompson, B.K. Soni, N.P. Weatherill (Eds.), *Handbook of Grid Generation*, CRC Press, January 1999.
- [83] M.J. Castro-Diaz, H. Borouchaki, P.L. George, F. Hecht, B. Mohammadi, Error interpolation minimization and anisotropic mesh generation, in: M. Morandi Cecchi, K. Morgan, J. Periaux, B.A. Schrefler, O.C. Zienkiewicz (Eds.), *Proceedings of 9th International Conference Finite Elements Fluids – New Trends and Applications*, Venezia, October 1995, pp. 139–148.
- [84] D.S. Malkus, T.J.R. Hughes, Mixed finite element methods in reduced and selective integration techniques: a unification of concepts, *Comput. Methods Appl. Mech. Eng.* 15 (1978) 63–81.
- [85] O.C. Zienkiewicz, P.N. Godbole, Viscous incompressible flow with special reference to non-Newtonian (plastic) flows, in: R.H. Gallagher et al. (Eds.), *Finite Elements in Fluids*, vol. 1, John Wiley & Sons, 1975, pp. 25–55, (Chapter 2)
- [86] T.J.R. Hughes, R.L. Taylor, J.F. Levy, A finite element method for incompressible flows, in: *Proceedings 2nd International Symposium on Finite Elements in Fluid Problems ICCAD*, Santa Margherita Ligure, Italy, 1976, pp. 1–6.
- [87] O.C. Zienkiewicz, P.N. Godbole, A penalty function approach to problems of plastic flow of metals with large surface deformation, *J. Strain Anal.* 10 (1975) 180–183.
- [88] O.C. Zienkiewicz, S. Nakazawa, The penalty function method and its applications to the numerical solution of boundary value problems, *ASME, AMD* 51 (1982) 157–179.
- [89] J.T. Oden, R.I.P. methods for Stokesian flow, in: R.H. Gallagher, D.N. Norrie, J.T. Oden, O.C. Zienkiewicz (Eds.), *Finite Elements in Fluids*, vol. 4, John Wiley & Sons, 1982, pp. 305–318 (Chapter 15)
- [90] O.C. Zienkiewicz, J.P. Vilotte, S. Toyoshima, S. Nakazawa, Iterative method for constrained and mixed approximation. An inexpensive improvement of FEM performance, *Comput. Methods Appl. Mech. Eng.* 51 (1985) 3–29.
- [91] O.C. Zienkiewicz, Y.C. Liu, G.C. Huang, Error estimates and convergence rates for various incompressible elements, *Int. J. Numer. Methods Eng.* 28 (1989) 2191–2202.
- [92] M. Fortin, Old and new finite elements for incompressible flow, *Int. J. Numer. Methods Fluids* 1 (1981) 347–364.

- [93] M. Fortin, N. Fortin, Newer and newer elements for incompressible flow, in: R.H. Gallagher, G.F. Carey, J.T. Oden, O.C. Zienkiewicz (Eds.), Finite Elements in Fluids, vol. 6, John Wiley & Sons, 1985, pp. 171–188 (Chapter 7).
- [94] M.S. Engleman, R.L. Sani, P.M. Gresho, H. Bercovier, Consistent vs. reduced integration penalty methods for incompressible media using several old and new elements, Int. J. Numer. Methods Fluids 2 (1982) 25–42.